IEEE Access
Multidisciplinary | Rapid Review | Open Access Journal

Received March 21, 2020, accepted April 1, 2020, date of publication April 7, 2020, date of current version April 21, 2020.

Digital Object Identifier 10.1109/ACCESS.2020.2986357

PALExo: A Parallel Actuated Lower Limb Exoskeleton for High-Load Carrying

TIANSHUO WANG, YANHE ZHU, (Member, IEEE), TIANJIAO ZHENG, DONGBAO SUI, SIKAI ZHAO, AND JIE ZHAO, (Member, IEEE)
State Key Laboratory of Robotics and System, Harbin Institute of Technology, Harbin 150001, China

Corresponding author: Yanhe Zhu (yhzhu@hit.edu.cn)

This work was supported in part by the National Key Research and Development Program of China under Grant 2018YFB1305400, and in part by the Joint Research Fund between the National Natural Science Foundation of China (NSFC) and Shen Zhen under Grant U1713201.

ABSTRACT The exoskeleton robots to assist load-carrying have received much attention in recent years. However, their load capacity and comfort are still insufficient. In this paper, we have developed a novel parallel actuated lower limb exoskeleton(PALExo), that addresses these problems. The novelty is that each limb of the exoskeleton is a 2-SPU underactuated parallel mechanism. Owing to the innovative series elastic module (SEM) with multi-segment stiffness, PALExo is compliant and comfortable for the wearer. The high load characteristic of the parallel structure increases the exoskeleton load capacity, and it can accommodate wearers of different heights without manual adjustment. A dynamic model of the exoskeleton was established, and in order to increase the robustness of the system, we designed a force control method based on sliding mode control and disturbance observer. Finally, the rationality and load-bearing effect of the exoskeleton were verified through a series of experiments including swing following, squatting and walking with loads.

INDEX TERMS Lower limb exoskeleton, parallel structure, sliding mode control, disturbance observer.

I. INTRODUCTION

Exoskeletons are powered robotic devices that can be worn by humans to enhance their strength or increase the efficiency of the rehabilitation therapy. The development of exoskeletons can be driven by many applications, including to improve the patient's recovery efficacy, to help paraplegic or quadriplegic people to regain locomotion ability, to provide additional power for walking or stair-climbing of people suffering from muscular weakness, and to empower healthy people to perform heavy loads carrying [1]. In this paper, we focus only on the lower limb exoskeletons for heavy load carrying.

There are some common criteria used to classify the exoskeletons. According to the proportion of active degrees of freedom(DOFs) in all DOFs, the exoskeleton can be divided into three types: passive, fully actuated and underactuated. According to the connection form of the mechanical structure, the exoskeleton also can be divided into three types: serial, parallel and series-parallel hybrid.

The associate editor coordinating the review of this manuscript and approving it for publication was Zheng Chen.

Hugh Herr classified exoskeletons and orthoses into devices that act in series and in parallel to a human limb [2], [3]. The exoskeletons in series with the human lower limb are mainly used to enhance the bounce and speed of the human, typical products of which include Springwalker [4], Power skip [5], Bionic Boots [6], and Kangoo-jumps [7]. Bionic Boots can propel the wearer forward at 24 mph, which is close to the top speed of 27 mph of world fastest runner Usain Bolt. An impact peak is observed in 15% of the experiments during running with Kangoo-jumps, compared to 96% of the experiments during running with running shoes. Wearing these exoskeletons in series with the human lower limb, the weight of the load is still entirely borne by the human leg. In contrast, exoskeletons in parallel with the human lower limb can transfer the weight of the load to the ground. Therefore, exoskeletons in parallel with the human limb are more conducive to load-bearing, and the exoskeletons discussed below in this paper also refer to this category. The most representative of this type of exoskeleton include BLEEX [8]–[10], HULC [11], HAL [12], [13], and XOS [14]. BLEEX's hip joints have three DOFs, knee joints have one DOF, and ankle joints have three DOFs, and four of

these DOFs are active. BLEEX can walk an average speed of 4.68 km/h with 34-kg load. HULC attains a maximum speed of 11 km/h and enables soldiers to carry load up to 91kg. These exoskeletons are all designed in series mechanical structure, which is similar to the layout of human limbs DOFs. This form of structure brings convenience to the DOFs arrangement and the joint actuator position control, but also brings some problems. Because this type of exoskeletons have similar DOFs arrangement with human's leg, many researchers choose to completely fix the lower limb of the exoskeleton to that of the wearer to ensure that the joints of the exoskeleton and the wearer's joints are always in the similar position or their rotation axes are collinear during the exercise. However, misalignment between the wearer's leg joints and device joints is an inevitable problem in exoskeletons with series structure. For example, the motion of the human knee is not a simple fixed-axis rotation, but a two-dimensional composite motion. It is difficult to simulate the motion with a simple combination of kinematic pairs. This misalignment may make the wearers feel uncomfortable, and even cause pain and great damage to wearers when joint drive torque is high [15].

Therefore, artificial polycentric knee joints utilizing various mechanisms are presented [16], such as an active artificial knee structured by a four bar-based polycentric linkage presented by Hyun [17]. However, this method also has a limitation that it is difficult to adapt to different wearers. On the other hand, to solve the problems caused by misalignment between the wearer's leg joints and device joints, there are some exoskeletons which have different DOFs arrangement from human limbs. Their legs are usually not fixed to the wearer's lower limbs, and their movements are different from those of the wearer's lower limbs when acting. The French HERCULE V3 [18] is developed by RB3D for weight carrying. It bundles with the wearer by backpack harness and flexible foot attachment system. HERCULE V3 weight 30kg and its payload is 40kg. The Japanese Honda Walker [19] is developed for walking assist, which is only 6.5kg weight. It is attached to the wearer by shoes and a seat which can support the weight of the wearer. Honda Walker innovatively placed the leg links of the device between the wearer's legs rather than the outside of legs. The different DOFs arrangement with the human lower limbs ensures the wearer's comfort. It is worth reminding that all of these exoskeletons mentioned above are designed in series mechanical structure, while the joint actuators in exoskeletons with series mechanical structure are required to be high-powered when the load is heavy. As a result, the limitation of joint actuators' power restricts the load ability of these exoskeletons. The exoskeletons with parallel mechanical structure provide an effective solution to the above this problem.

Parallel structures have been applied in a wide variety of fields in situations where higher accuracy, speed, stiffness and lower effective inertia are needed [20]–[23]. The advantage inherent to Parallel structures makes this type of mechanical structure suitable for exoskeleton limb applications [24].

At present, researchers have applied parallel structures to exoskeletons, prior works include wearable wrist, ankle, and shoulder devices, for example the RiceWrist [25], Anklebot [26], and BONES [27]. BONES uses a parallel mechanism inspired by the human forearm to allow naturalistic shoulder movements. It uses four linear actuators to control the 3DoF of the shoulder. The prior works almost focus on fully-driven parallel structures to achieve purely rotational or spherical motion of a single joint, and they are mostly used for medical rehabilitation. However, fully actuated exoskeletons must be bulky and complex.

In summary, most of the existing exoskeletons for load bearing are based on series mechanical structure. However, there are some problems with this type of exoskeletons: 1. the load-bearing capacity is limited by the power and weight of the actuator; 2. it is difficult to perfectly adapt to wearers of different heights, which brings comfort issues. To solve the above problems, we present a novel design of an underactuated lower limb exoskeleton based on parallel structures in this paper, which is more suitable for load-bearing. And because of its different DOFs arrangement with the lower limbs of human body, the movement of the wearer's feet relative to the torso can be formed by the parallel structure, so only the torso and feet of the wearer are bundled with the exoskeleton. And because the exoskeleton is not completely fixed to the human leg, there will not be discomfort and joint damage due to misalignment between the wearer's leg joints and device joints even if with wearers of different heights.

We developed an exoskeleton prototype, proposed a control method suitable for the exoskeleton based on sliding mode control and disturbance observer, and the rationality and load-bearing effect of the exoskeleton were verified through a series of experiments. This paper provides a new idea for exoskeleton research.

The remainder of this paper is organized as follows: after the design of parallel actuated lower limb exoskeleton (PALExo) is described in Section II, a force following control method for PALExo based on sliding mode control and disturbance observer is presented in Section III. The developed device is verified in experiments in Section IV. Finally, Section V concludes the paper and propose directions for possible future work.

II. DESIGN OF PALEXO

A. MECHANICAL DESIGN

While rare in exoskeleton designing, we proposed a non-anthropomorphic architecture with four active degrees of freedom. The DOFs arrangement is shown in Fig.1(b). PALExo has two chains per leg, and there are three pairs per chain, each chain has one passive universal pair, one active prismatic pair and one passive spherical pair. In addition, a passive revolute pair was added on the back of PALExo to fulfill the swing of hip during human walking. The main function of this exoskeleton we developed is load-bearing. With this DOFs arrangement, we take advantage of the low effective inertia and high load capacity of parallel structure,

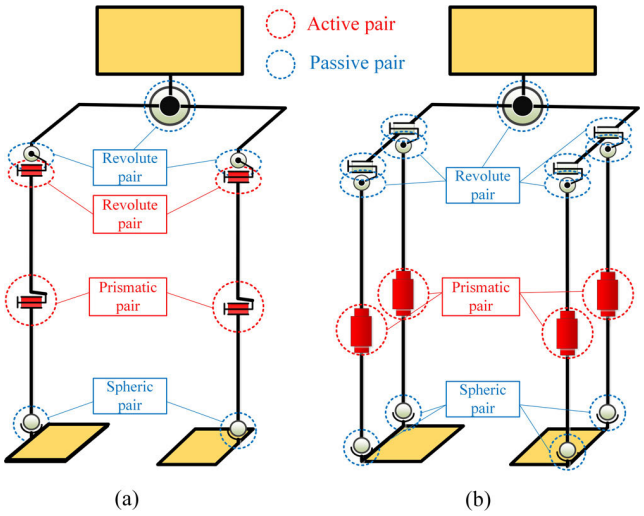

FIGURE 1. DOFs arrangement of an exoskeleton with series structure and PALExo.

FIGURE 2. The composition of the exoskeleton mechanical system and the prototype with a wearer. PALExo can be mainly divided into three parts: the upper body, legs, and shoes. Each leg of the exoskeleton contains two active telescopic rods, which connect the upper body and the shoes through the hook and hinge at the end. The wearer in the picture is 188mm tall and weighs 79kg.

which improves the load capacity of the exoskeleton. And because the exoskeleton resists the gravity of itself and the load when it works, it mainly plays a role in supporting in the vertical direction, so we choose the prismatic pair as active DOFs. In order to balance a part of the torque formed by the weight in the sagittal plane and reduce the burden on the wearer's waist when carrying a load, we chose two active electric cylinders in one leg to form a parallel structure instead of one.

For comparison, we also propose a DOFs arrangement scheme for the exoskeleton with series structure. Taking an exoskeleton developed by our group as an example [28], its DOFs arrangement is shown in Fig.1(a). There are 6 DOFs in one leg of this exoskeleton, including 2 DOFs for the hip joint, 1 DOF for the knee joint, and 3 DOFs for the ankle joint. There are 2 actuators in one leg of the exoskeleton: flexion and extension movement of hip joint and knee joint.

The movement of the human body is mainly concentrated in the sagittal plane, so in the study of exoskeletons, the movement in the sagittal plane is often more concerned. In the sagittal plane, the parallel structure of each leg of PALExo can be considered as a four-bar linkage, where two rods are telescoping as active joints. When the actuators are locked, there exists one passive DOF in this structure, which is driven by the wearer's hip joint, knee joint and ankle joint together. However, the passive DOF of the exoskeleton with series structure has to be drived by wearer's ankle joint independently. And human ankle joints are not so strong compared to hip and knee joints. Therefore, compared with the exoskeleton with series structure, the parallel structure enables PALExo to bring more comfort to the wearer.

According to the arrangement of DOFs mentioned above, we developed the exoskeleton with parallel structure, named PALExo, as shown in Fig.2. Its weight, including the battery, is approximately 27.8kg. It allows the wearer to walk at a maximum speed of 7km/h, and can accommodate wearers with a height of 160cm to 190cm without manual adjustment.

Although the architecture of PALExo is different from human leg, PALExo can still follow the motion trail of the wearer's leg by coupling movements of passive revolute joints and linear actuators together. Because each chain of the parallel structure has 6 DOFs, the shoes fixed with the ends of two chains also has 6 DOFs, that makes the legs of PALExo be able to meet the requirements of the wearer's legs for DOFs. The process of PALExo's single leg following the wearer's leg movement is shown in Fig.3.

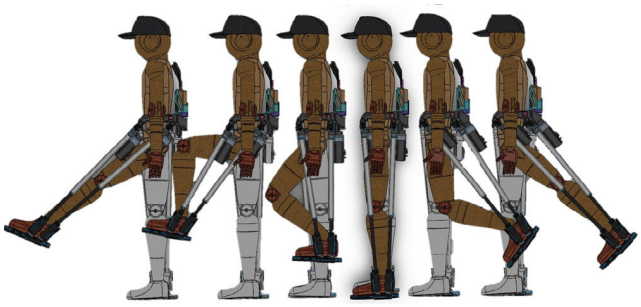

FIGURE 3. The process of PALExo's single leg following the wearer's leg movement.

In order to adapt to wearers of different heights, the leg length of the exoskeleton will be adjusted according to the wearer's leg length, thanks to the two telescopic cylinders on each leg of PALExo, as shown in Fig.4. And the control target of the active joint control method we use is force rather than position, which makes it unnecessary for us to adjust the control parameters according to the wearer's height.

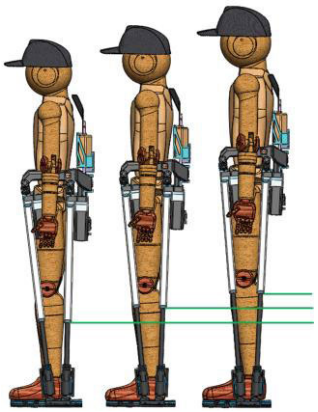

FIGURE 4. How does PALExo adapts to wearers of different heights.

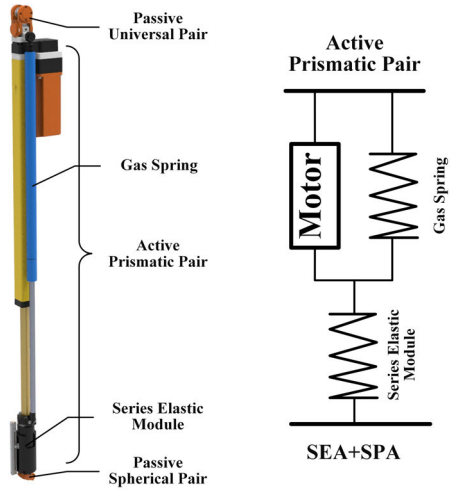

FIGURE 5. Chain of serial-parallel architecture.

As shown in Fig.2, PALExo can be mainly divided into three parts: waist and back part, legs, and shoes. As mentioned above, per leg of PALExo has a parallel structure containing two chains. And there are three pairs per chain: one passive universal pair, one active prismatic pair and one passive spherical pair, as shown in Fig.5. The active prismatic pair consists of three parts: an electric cylinder, a gas spring installed in parallel with the electric cylinder, and a series elastic module installed in series with the electric cylinder.

Electric cylinder and gas spring form a parallel elastic actuator(SPA). The gas spring can provide a constant supporting force, which can reduce the burden on the motor of the electric cylinder. The idea is that the parallel gas spring generates part of the force required to support the load and the motor only provides the others. Parallel gas springs can increase the maximum output force that the actuator can provide. Depending on the load, the gas spring can be replaced with a different model or removed.

We designed a series elastic module (SEM) installed in series with the electric cylinder, as shown in Fig.6. During the exoskeleton walking, the legs frequently switch between

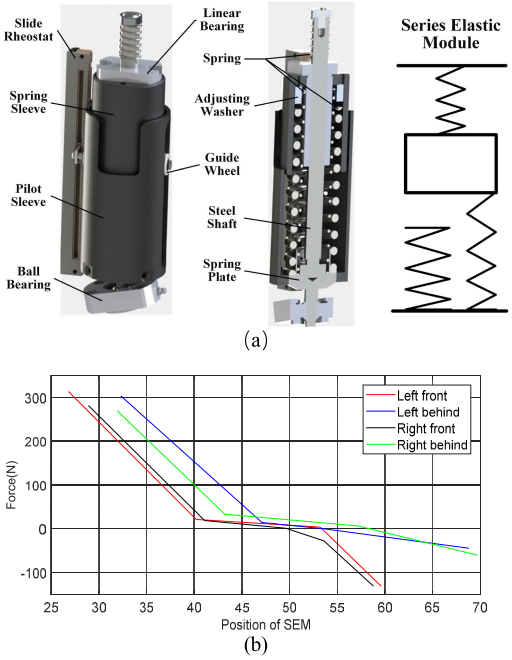

FIGURE 6. Series elastic module(SEM). (a) The mechanical structure of SEM. (b) Stiffness identification result of four SEM.

the swing phase and the stance phase, and the required force of actuators in the two phases are very different. So it is difficult for a SEM with constant stiffness to adapt to both situations. To overcome this problem, the SEM we designed consists of two springs with smaller stiffness and one spring with biger stiffness, and will show three different stiffness levels depending on the amount of compression. When the leg of the exoskeleton is in the swing phase, it is mainly the two smaller springs of the SEM that work. On the contrary, when the leg of the exoskeleton is in the stance phase, it is mainly the larger spring of the SEM that works. In addition, the amount of compression of each SEM can be measured by a slide rheostat. There are three main purposes for introducing this SEM.

(1) Increase the limit speed of exoskeleton. Only the two smaller springs work when PALExo's leg is in the swing phase. Under certain circumstances, when wearer's leg instantaneously moving faster than PALExo's limit speed, the wearer still has a certain range of safe movement due to compression of the springs, instead of suffering an intense impact from the exoskeleton.

(2) The SEM can act as a buffer. The larger spring mainly works when the leg of the exoskeleton is in the stance phase, which can reduce the impact of landing. In addition, when exoskeleton's leg is in the process of landing, the spring can compress and store the potential energy and release the stored energy when the leg lifting, which can increase the utilization ratio of energy.

(3) The interaction force between the human foot and PALExo can be indirectly obtained by measuring the compression of the SEM, using a sliding rheostat.

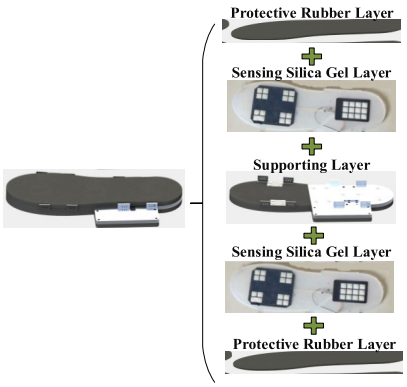

FIGURE 7. The structure of the shoe.

We developed a shoe with contact switches, as shown in Fig.7. The shoe is divided into five layers: the middle supporting rubber structure, the top and the lowest two layers of protective rubber pad, and the two silica gel layers with contact switches inside. The contact condition between the wearer and the shoe can be measured with upper contact switches, and the contact condition between the exoskeleton and the ground is measured by the lower one. This shoe can detect in real time whether the legs of the exoskeleton are in the stance phase or the swing phase.

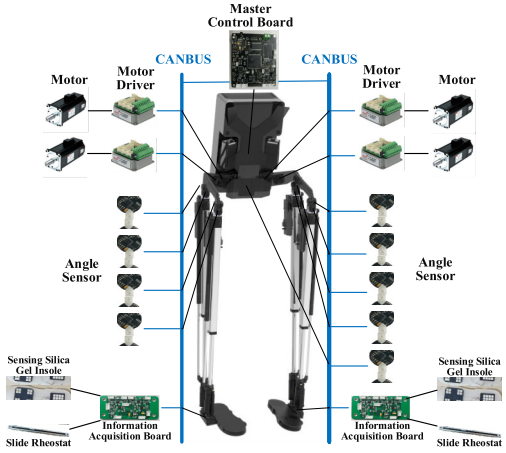

FIGURE 8. The networked control system of PALExo.

B. DESIGN OF ELECTRICAL SYSTEM

For supporting the control algorithm and achieve high-speed real-time control, we set up the electrical system as shown in Fig. 8. We developed a master control board with a DSP TMS320F28335 as the CPU. Since there are a group of sensors and four motors, it is almost impossible to route all signal wires directly to the master control board. Thus, we chose CANBUS for communication. The system consists of two communication line, which are distributed in the two legs of PALExo. Besides the master control board, there are 15 nodes in the system, including 4 motor drivers that drive motors and collect motor signals, 9 angle sensors that measure hinge angles, and 2 information collection boards that collect the foot contacting information and position signal of the slide rheostat. With the system, we can easily add or remove slave nodes and reduce the complexity and difficulty of wiring. The baud rate of the CAN bus is 1M/s, and the controller updates at 250Hz.

III. CONTROL OF PALEXO

In the process of walking, the legs of the exoskeleton frequently switch between the swing phase and the stance phase. In the swing phase, the actuator only needs to provide the force required for changing the kinestate of a single leg, meanwhile the stance leg needs to support weight of the exoskeleton. So, we controlled the actuators on swing leg or stance leg with two different control strategies.

We control the four actuators independently, the control block diagram of each actuator is shown in Fig.9.

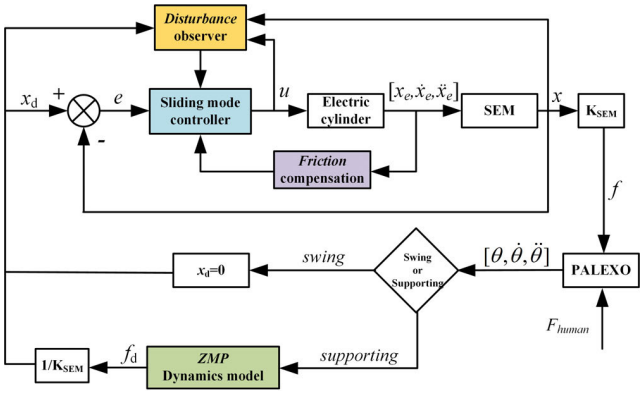

FIGURE 9. Control block diagram of each chain.

The control strategy on the actuator of the exoskeleton is divided into two parts: obtaining the value of target force and controlling the motor to follow the target force. 1. In order to obtain the value of target force, we judge whether the leg is in the stance phase or the swing phase according to the current state of sensors. When the leg is in the swing phase, our control goal is to make the exoskeleton's leg follow the wearer's swing leg, and the exoskeleton doesnot affect the motion of the wearer's swing leg, that is the human-machine interaction force of the swing leg is 0. So the target force of the swing leg is 0. If it is in the swing phase, the target force is considered to be zero. Otherwise, the target output force is calculated according to dynamic model proposed in Section III-A. 2. We adjust the motor output torque to follow the target force. The value of the motor output torque is composed of three parts: the sliding mode control amount based on the nominal model, the friction compensation identified by genetic algorithm (GA), and the disturbance compensation obtained by the observer. In this section, we will introduce dynamic model of stance legs, sliding mode control based on nominal model, disturbance observer, and friction identification base on GA respectively.

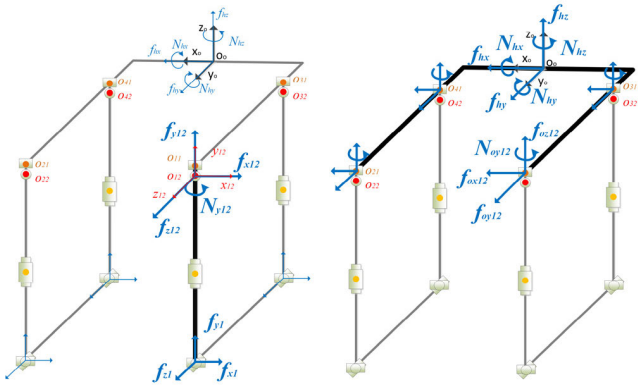

FIGURE 10. The simplified dynamic model of the exoskeleton legs. The exoskeleton can be considered as a structure consisting of four chains, and each chain has one actuator.

A. DYNAMIC ANALYSIS FOR PALExo

In the stance phase, the dynamic model of the exoskeleton can be considered as a structure consisting of four chains, as shown in Fig.10.

Analyzing the force acting on PALExo, it can be found that regardless of the phase of the legs (stance phase or swing phase), the external force is derived from three parts. First part is gravity acting on the center of mass. The second part is the six-dimensional force and torque acting on the upper body of exoskeleton from the human body, shown as f_{hx}, f_{hy}, f_{hz}, N_{hx}, N_{hy}, N_{hz} in Fig. 10. The third part is a three-dimensional force acting on the end of each chain from human foot or the ground, shown as f_{x1},f_{y1},f_{z1} in Fig. 10. (Each end of the chain is a ball hinge, so there is no torque). Among them, f_{y1} is the force acting on the end of the chain and in the direction of the telescopic rod, that is the target force of our control algorithm. Therefore, in order to obtain the target force, we establish a dynamic model suitable for the legs in the stance phase and in the swing phase. Therefore, we can establish a unified dynamic model of PALExo, which is suitable for both the stance phase and the swing phase.

In order to simplify the dynamic model, we assume that point O12 coincides with point O11.

The process of establishing the dynamic model is divided into two parts: 1. The force analysis of each chain of the parallel structure is performed to obtain the force between the chain and the upper body f_{oxn2},f_{oyn2},f_{oxn2}, N_{oyn2}, $n = 1, 2, 3, 4$ represented by f_{yn}, $n = 1, 2, 3, 4$. 2. The force analysis of the upper body of the exoskeleton is performed to obtain the target supporting force at the end of the chain f_{yn}, $n = 1, 2, 3, 4$. 3. Finally, the human-machine interaction force and acceleration of the back are taken as 0. Since there are six equations, but only four unknown variables, the equations need to be selected based on the degree of importance.

(1) The force analysis of each chain of the parallel structure is performed. We analyze the force acting on each chain in the chain coordinate system, taking the No.1 chain in Fig. 10 as an example. f_{x1}, f_{z1} and N_{y12} can be calculated from the Euler equation.

$$f_{x1} = (J_{zo12} \cdot \propto_{zo12} - N_{m1z}) / R_{oe} \quad (1)$$

$$f_{z1} = (J_{xo12} \cdot \propto_{xo12} - N_{m1x}) / R_{oe} \quad (2)$$

$$N_{y12} = J_{yo12} \cdot \propto_{yo12} - N_{m1y} \quad (3)$$

where, N_{y12} is the constraint torque from the upper body of PALExo around the chain, J_{xo12}, J_{yo12}, J_{zo12} is the moment of inertia of the rod rotating around the three coordinate axes, $\propto_{xo12}$, $\propto_{yo12}$, $\propto_{zo12}$ is the angular acceleration of the rod rotating around the three coordinate axes, N_{m1x}, N_{m1y}, N_{m1z} is the torque of gravity on the three coordinate axes, R_{oe} is the length of the chain.

From Newton equation, we get:

$$f_{x12} = m_1 \cdot a_{xo12} - m_1 \cdot g_{xo12} - f_{x1} \quad (4)$$

$$f_{y12} = m_1 \cdot a_{yo12} - m_1 \cdot g_{yo12} - f_{y1} \quad (5)$$

$$f_{z12} = m_1 \cdot a_{zo12} - m_1 \cdot g_{zo12} - f_{z1} \quad (6)$$

where, f_{x12}, f_{y12}, f_{z12} is the constraint force from the upper body of PALExo along three coordinate axes, m_1 is the mass of the rod, a_{xo12}, a_{yo12}, a_{zo12} is the acceleration of the rod along three coordinate axes, g_{xo12}, g_{yo12}, g_{zo12} is the component of the acceleration of gravity in the three coordinate axes.

Then, we can obtain the restraint force and torque from the chain rod acting on the upper body of PALExo f_{ox12},f_{oy12},f_{oz12},N_{oy1}(expression with f_{y1}), and other chains are the same.

(2) The force analysis of the upper body of the exoskeleton is performed. We analyze the force acting on the upper body of PALExo in the inertial coordinate system.

$$f_{hx} + f_{ox12} + f_{ox22} + f_{ox32} + f_{ox42} = m_0 a_{xo} \quad (7)$$

$$f_{hy} + f_{oy12} + f_{oy22} + f_{oy32} + f_{oy42} = m_0 a_{yo} \quad (8)$$

$$f_{hz} + f_{oz12} + f_{oz22} + f_{oz32} + f_{oz42} - m_0 g = m_0 a_{zo} \quad (9)$$

$$N_{hx} + \sum_{n=1}^{4} N_{nx} + \sum_{n=1}^{4} N_{oyn}^{x} + N_{m0gx} = J_{x0} \propto_{x0} \quad (10)$$

$$N_{hy} + \sum_{n=1}^{4} N_{ny} + \sum_{n=1}^{4} N_{oyn}^{y} + N_{m0gy} = J_{y0} \propto_{y0} \quad (11)$$

$$N_{hz} + \sum_{n=1}^{4} N_{nz} + \sum_{n=1}^{4} N_{ozn}^{z} = J_{z0} \propto_{z0} \quad (12)$$

where, $N_{nx} = f_{oyn2} \cdot z_n + f_{ozn2} \cdot y_n$, $N_{ny} = f_{ozn2} \cdot x_n + f_{oxn2} \cdot z_n$, $CN_{nz} = f_{oyn2} \cdot x_n + f_{oxn2} \cdot y_n$, $n = 1, 2, 3, 4$.

(x_n, y_n, z_n) is the coordinates of the origin of the No.n chain coordinate system in the inertial coordinate system, m_0 is the mass of the upper body of PALExo, a_{xo}, a_{yo}, a_{zo} is the acceleration of the upper body along three coordinate axes, N_{oyn}^{x}, N_{oyn}^{y}, N_{oyn}^{z} is the component of N_{oyn} in the three coordinate axes, N_{m0gx}, N_{m0gy} is the torque of gravity on the coordinate axes, J_{xo}, J_{yo}, J_{zo} is the moment of inertia of the upper body rotating around the three coordinate axes, $\propto_{xo}$, $\propto_{yo}$, $\propto_{zo}$ is the angular acceleration of the upper body rotating around the three coordinate axes.

(3) Considering the wearing comfort, we might as well set the human-machine interaction force on the upper body to zero (i.e., $f_{hx} = f_{hy} = f_{hz} = N_{hx} = N_{hy} = N_{hz} = 0$). In order for the exoskeleton to compensate for the load and its own gravity, we hope 6 accelerations of the center of mass to be zero. Since the exoskeleton has only four active DOFs and cannot satisfy six equations at the same time, the system is an underactuated system. The exoskeleton cannot make the 6 accelerations of the center of mass zero simultaneously just relying on itself. Considering the importance of acceleration in different directions or angles and the comfort of the wearer, $a_{zo} = \propto_{x0} = \propto_{y0} = \propto_{z0} = 0$ is taken when the two legs of exoskeleton are in stance phase, and the other two directions are balanced by the wearer only. When only one leg of the exoskeleton is in stance phase, $a_{zo} = \propto_{x0} = 0$ is taken.

B. SLIDING MODE CONTROL

According to the above dynamic analysis of PALExo, we can obtain the target force of each actuator. Hereafter, in order to control the motor to follow the target force, we present a force control method based on sliding mode control.

The model of each electric cylinder system can be formulated as follows:

$$u = \mathrm{M}(\mathrm{x}) \cdot \ddot{x} + B(x, \dot{x}) \cdot \dot{x} + f(x, \dot{x}) + G(q) + d(t) \quad (13)$$

where $M(x)$ indicates the mass of electric cylinder, $B(x, \dot{x})$ indicates the Coriolis and Centrifugal force coefficient, $f(x, \dot{x})$ indicates the frictional force, $G(q)$ indicates the gravitational force, $d(t)$ indicates disturbances, u indicates the input torque.

Let $e = x_d - x$ be the position error, where x_d is the position command signal. We design the sliding mode surface as:

$$s = \dot{e} + ce \quad (14)$$

then introducing (13) into (14), we get $\dot{s}$:

$$\dot{s} = \ddot{e} + c\dot{e} = c\dot{e} + \ddot{x}_d - \ddot{x} \quad (15)$$

$$\dot{s} = c\dot{e} + \ddot{x}_d - \frac{1}{M}(u - B \cdot \dot{x} - f - G - d(t)) \quad (16)$$

Approach law can be used to improve the dynamic quality of approaching motion.

We design the exponential approach law as:

$$\dot{s} = -\eta \cdot sgn(s) - ks \quad (17)$$

According to (16), the control law can be designed as follows:

$$u = M(c\dot{e} + \ddot{x}_d + \eta \cdot sgn(s) + ks) + B \cdot \dot{x} + f + G + d(t) \quad (18)$$

We consider modeling errors, parameter changes, and other uncertainties as external disturbance $d(t)$. Taking d_c instead of $d(t)$, the control law is expressed as follows

$$u = M(c\dot{e} + \ddot{x}_d + \eta \cdot sgn(s) + ks) + B \cdot \dot{x} + f + G + d_c \quad (19)$$

Then the actual sliding mode approach law is

$$\dot{s} = -\eta \cdot sgn(s) - ks - \frac{1}{M}(d(t) - d_c) \quad (20)$$

We define Lyapunov function as follows:

$$V = \frac{1}{2}s^2 \quad (21)$$

and we get the derivative of Lyapunov function as:

$$s\dot{s} = -\eta \cdot |s| - ks^2 - s\frac{1}{M}(d(t) - d_c) \quad (22)$$

By selecting d_c we can ensure the stability of the control system, that is, to meet the sliding mode arrival conditions. We assume

$$d_L \le d(t) \le d_U \quad (23)$$

where d_L and d_U, respectively, are the lower and upper bound of the disturbance.

Letting $d_1 = (d_U - d_L)/2$ and $d_2 = (d_U + d_L)/2$, we can design d_c that meets the above conditions as:

$$d_c = d_2 - d_1 sgn(s) \quad (24)$$

then the control law can be expressed as follows:

$$u = M(c\dot{e} + \ddot{x}_d + \eta \cdot sgn(s) + ks) + B \cdot \dot{x} + f + G + d_2 - d_1 sgn(s) \quad (25)$$

We simulate the system with the above-mentioned control law by MATLAB/SIMULINK. We take the target position $x_d = sint$ and the disturbance $d(t) = 0.1\cos(5t + \pi/2) + 0.02$. The actual values of system parameters are taken respectively as $M = 1.5$, $B = 0.1$, $f = 5$, $G = 15$, and their nominal values are taken respectively as $M_0 = 1.4$, $B_0 = 0.15$, $f_0 = 3$, $G_0 = 14$, $d_0 = 0.15$. Taking $d_L = -0.12$, $d_U = 0.12$, $\eta = 2.2$, $k = 10$, the simulation results are shown in Fig.11.

It can be seen from the simulation results that the input signal of the control system has no obvious jitter, and the target position can be tracked quickly and accurately. The maximum value of the position tracking error is about 3.8 mm. However, the position error always exists and is larger than 3 mm, with an average value of about 3.5 mm.

C. DISTURBANCE OBSERVER

It can be seen from the above equations that the switching gain of the control amount is related to d_1, that is, the difference between the upper and lower bound of disturbance $d_U - d_L$ directly affects the switching range of the control amount. However, the upper and lower bounds of disturbance are not easy to give in practical applications. In order to ensure the stability of the system, a large value is often selected, which leads to large-scale jitter of the control system. To reduce this jitter, a reasonable estimate of the disturbance is needed, and then a sliding observer control based on the disturbance observer is proposed below.

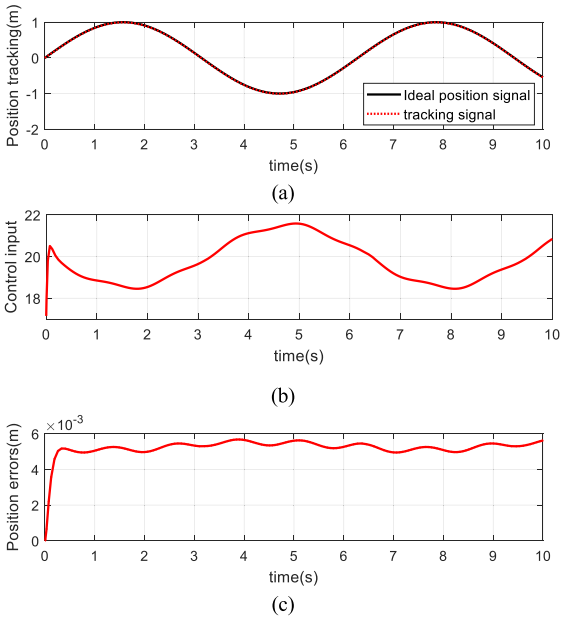

FIGURE 11. Simulation results of sliding mode robust control based on approach law. (a) Position tracking curve. (b) Input signal. (c) Position errors.

We design an observer for disturbance $d\ (t)$ as:

$$\dot{d}_e = k_1 \frac{1}{M}\tilde{\varphi} \tag{26}$$

$$\dot{\varphi} = \frac{1}{M}(d_e + k_2\tilde{\varphi} - u + B\cdot\dot{x} + f + G + M\ddot{x}_d) \tag{27}$$

where the d_e and φ indicate the estimated value of $d\ (t)$ and $\dot{e}$, respectively. $\tilde{\varphi} = \dot{e} - \varphi$, the gain $k_1, Ck_2 > 0$.

Lyapunov function is defined as

$$V = \mathrm{V}_1 + \mathrm{V}_2 = \frac{1}{2}s^2 + \frac{1}{2k_1}\tilde{d}^2 + \frac{1}{2}\tilde{\varphi}^2 \tag{28}$$

where $\mathrm{V}_1 = s^2/2$, $\mathrm{V}_2 = \tilde{d}^2/2k_1 + \tilde{\varphi}^2/2$, $\tilde{d} = d - d_e$.

Then the derivative of V_2 is

$$\dot{V}_2 = \frac{1}{k_1}\tilde{d}\dot{\tilde{d}} + \frac{1}{2}\tilde{\varphi}\dot{\tilde{\varphi}} = \frac{1}{k_1}\tilde{d}(\dot{d} - \dot{d}_e) + \tilde{\varphi}(\ddot{e} - \dot{\varphi}) \tag{29}$$

Assuming the disturbance is a slow time-varying signal, we can consider $\dot{d} = 0$. Introducing (26) and (27) into (29), we get

$$\dot{V}_2 = -\frac{1}{k_1}\tilde{d}k_1\frac{1}{M}\tilde{\varphi} + \tilde{\varphi}[\ddot{x}_d - \ddot{x} - \frac{1}{M}(d_e + k_2\tilde{\varphi} - u + B\cdot\dot{x} + f + G + M\ddot{x}_d)] \tag{30}$$

According to (13), $\dot{V}_2$ can be written as

$$\dot{V}_2 = -\frac{1}{M}\tilde{d}\tilde{\varphi} + \tilde{\varphi}[\ddot{x}_d - \frac{1}{M}(u - B\cdot\dot{x} - f - G - d) - \frac{1}{M}(d_e + k_2\tilde{\varphi} - u + B\cdot\dot{x} + f + G + M\ddot{x}_d)] \tag{31}$$

Rearranging (31), we get

$$\dot{V}_2 = -\frac{1}{M}\tilde{d}\tilde{\varphi} + \tilde{\varphi}\left[\frac{1}{M}\left(\tilde{d} - k_2\tilde{\varphi}\right)\right] = -\frac{1}{M}k_2\tilde{\varphi}^2 \le 0 \tag{32}$$

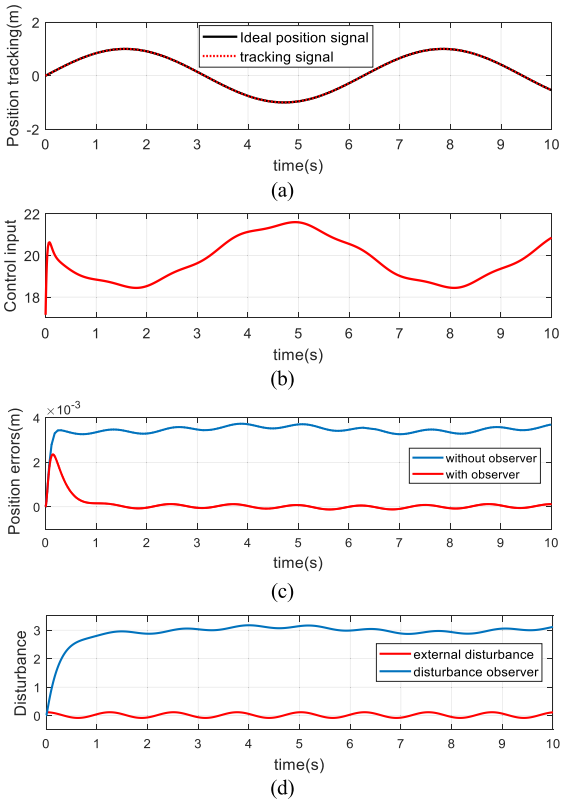

FIGURE 12. Simulation results of sliding mode robust control based on disturbance observer. (a) Position tracking curve. (b) Input signal. (c) Position errors with or without disturbance observer. (d) Disturbance observation curve.

Because $\mathrm{V}_1 \le 0$, $\dot{V} = \dot{V}_1 + \dot{V}_2 \le 0$. Then the control law can be rewritten in the format of

$$u = M\ (c\dot{e} + \ddot{x}_d + \eta\cdot sgn\,(s) + ks) + B\cdot\dot{x} + f + G + d_e + d_c \tag{33}$$

Adding the observed d_e to compensate for the disturbance, d_e can be given a smaller value, which reduce the jitter of the system. To make the jitter smaller, the symbolic function $sgn\ (s)$ in the control law can be replaced with $s/(\,|s| + \delta)$, and then the control law is rewritten as

$$u = M\left(c\dot{e} + \ddot{x}_d + \eta\cdot\frac{s}{|s| + \delta} + ks\right) + B\cdot\dot{x} + f + G + d_e + d_2 - d_1\frac{s}{|s| + \delta} \tag{34}$$

We simulate the system with the above-mentioned control law by MATLAB/SIMULINK. We take the target position $x_d = sint$ and the disturbance $d\ (t) = 0.1\cos(5t + \pi/2) + 0.02$. The actual values of system parameters are taken respectively as $M = 1.5$, $B = 0.1$, $f = 5$, $G = 15$, and their nominal values are taken respectively as $M_0 = 1.4$, $B_0 = 0.15, f_0 = 3$, $G_0 = 14, d_0 = 0.15$. Taking $d_L = -0.05$, $d_U = 0.05, k_1 = 1000$, $k_2 = 200$, $\eta = 2.2$, $k = 10$, the simulation results are shown in Fig.12.

It can be seen from the simulation results that the input signal of the control system has no obvious jitter, and the target

position can be tracked quickly and accurately. The maximum value of the position tracking error is about 2.4 mm.

After the system is stabilized, the position error always swings around 0, and the swing amplitude is about 0.12 mm. The disturbance observation curve shows that the observed disturbance includes not only the external input interference $d(t)$, but also the modeling error of the system model parameters M, B, f, G. The average value of the observed disturbance is about 3 larger than the external input disturbance, which is exactly the sum of the modeling error Δ f and ΔG, which are the two constant values in the control law. It shows that the addition of the disturbance observer in the control law can compensate for both external disturbance and system modeling error.

D. FRICTION IDENTIFICATION BASED ON GENETIC ALGORITHM

All parameters in the control law can be theoretically calculated to obtain a nominal value, except for the friction force f. In order to improve motion accuracy, the friction of the electric cylinder in the exoskeleton chain is usually relatively large, which has a great influence on the control system. To obtain a more accurate estimate of the friction force, we use the genetic algorithm (GA) to identify it.

The static friction phenomenon exists in the electric cylinder at low speed. Hence, the friction force is identified by the LuGre friction model.

$$F = \left[F_c + (F_s - F_c)\, e^{-\left(\frac{\dot\theta}{V_s}\right)^2}\right] sgn\left(\dot\theta\right) + \alpha\dot\theta \tag{35}$$

where F_c, F_s, α, V_s are static friction parameters, F_c is coulomb friction, F_s is static friction, α is the coefficient of viscous friction, V_s is switching speed. When the servo system is running in the forward and reverse rotational speeds, the static parameters of the friction torque are usually different values. When $\dot\theta > 0$, they are F_c^+, F_s^+, α^+, V_s^+; When $\dot\theta < 0$, they are F_c^-, F_s^-, α^-, V_s^-, then the friction torque can be expressed as

$$F = \begin{cases} \left[F_c^+ + \left(F_s^+ - F_c^+\right) e^{-\left(\frac{\dot\theta}{V_s^+}\right)^2}\right] sgn\left(\dot\theta\right) \\ \quad +\alpha^+\dot\theta, \qquad \dot\theta > 0 \\ \left[F_c^- + \left(F_s^- - F_c^-\right) e^{-\left(\frac{\dot\theta}{V_s^-}\right)^2}\right] sgn\left(\dot\theta\right) \\ \quad +\alpha^-\dot\theta, \qquad \dot\theta < 0 \end{cases} \tag{36}$$

According to the physical model of the electric cylinder, when the electric cylinder is moving at a constant speed, the input torque of the motor is equal to the frictional force. Taking 50 sets of motor speed from −3000r/min to 3000r/min, the motor torque is recorded during the whole stroke, whose average value can be considered as the friction value F^i.

The identification of the friction parameter vector x is taken as an individual, and the identification value of the static friction parameters obtained by each iteration of the GA are

$$\hat{x}_m = [\hat{F}_c^+ \quad \hat{F}_s^+ \quad \hat{\alpha}^+ \quad \hat{V}_s^+ \quad \hat{F}_c^- \quad \hat{F}_s^- \quad \hat{\alpha}^- \quad \hat{V}_s^-], \quad m = 1, 2, \ldots, M \tag{37}$$

where M is the population size. According LuGre friction model, corresponding friction torque identification value $\hat{F}^i$ can be calculated. Identification error is defined as

$$e_i = F^i - \hat{F}^i, \quad i = 1, 2, \ldots, 64 \tag{38}$$

The objective function of the GA is taken as

$$J_m = \frac{1}{2}\sum_{i=1}^{N} e_i^2, \quad m = 1, 2, \ldots, M \tag{39}$$

The individual fitness function is selected as follows

$$\begin{cases} C_{max} = max\,\{J_m\} \\ f_m = C_{max} - J_m \end{cases}, \quad m = 1, 2, \ldots, M \tag{40}$$

The selective operation takes a random sampling selection method that preserves the optimal individual. Crossover operation uses uniform crossover with a crossover probability of 0.9. The mutation operation uses a Gaussian mutation operator, and the mutation probability is adaptively adjusted with evolutionary algebra, as follows:

$$P_m(g) = 0.1 - (0.1 - 0.001)\frac{g}{G} \tag{41}$$

where g is the current genetic algebra, and G is the maximum number of generations.

Taking the population size $M = 1000$, G = 50000 and the parameter search range $F_c \in [0, 300]$, $F_s \in [0, 300]$, $\alpha \in [0, 1]$, $V_s \in [0, 1000]$, we get the objective function value as 298.666 with number of generations. The objective function curve during evolution is shown in Fig.13.

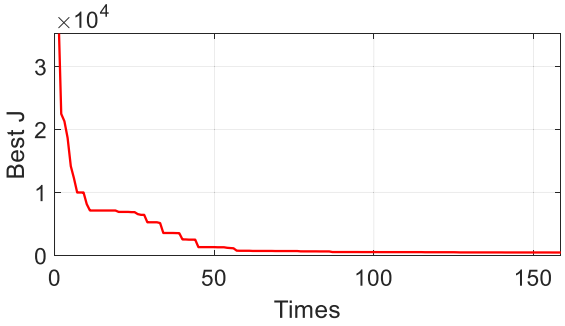

FIGURE 13. The objective function curve during evolution.

The identification value of the friction parameter obtained are $F_c^+ = 146.551$, $F_s^+ = 87.302$, $\alpha^+ = 0.0253$, $V_s^+ = 451.965$, $F_c^- = 153.038$, $F_s^- = 88.462$, $\alpha^- = 0.0210$,

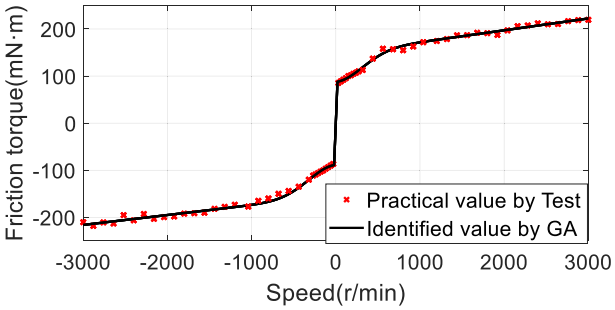

FIGURE 14. The identified friction torque curve.

$V_s^- = 455.247$, and then the identified friction torque is

$$F = \begin{cases} \left[146.551 + (87.302 - 146.551)\, e^{-\left(\frac{\dot{\theta}}{451.965}\right)^2}\right] \\ \quad \cdot sgn\left(\dot{\theta}\right) + 0.0253\dot{\theta}, \quad \dot{\theta} > 0 \\ \left[153.038 + (88.462 - 153.038)\, e^{-\left(\frac{\dot{\theta}}{455.247}\right)^2}\right] \\ \quad \cdot sgn\left(\dot{\theta}\right) + 0.021\dot{\theta}, \quad \dot{\theta} < 0 \end{cases} \tag{42}$$

The identified friction torque curve is shown in Fig.14.

IV. EXPERIMENT

In this section, we implemented a series of experiments to verify the rationality of the device and the effect of the control algorithm. The wearer is a 187-cm tall male weighing 79kg and aged 27.

FIGURE 15. Test process diagram. The test shows that the structure and control strategy can meet the requirements of normal activities.

A. BASIC ACTIVITIES TEST

With the control strategy mentioned above, we controlled PALExo to achieve basic functionality. In order to verify the rationality of structure and the range of motion, PALExo was operated to perform a series of activities, as shown in Fig.15. The test shows that the structure and control strategy can meet the requirements of normal activities.

B. FRICTION FORCE COMPENSATION EXPERIMENT

In order to verify the accuracy of the electric cylinder friction identification, we carried out the friction compensation experiment of the electric cylinder, which implemented reciprocating motion at a speed of approximately 0.2m/s. The motor is controlled to work in the torque loop. The torque command is the friction compensation value identified above in Section III. The SEM is grasped by human hand to drive the electric cylinder to reciprocate. Then compression amount of the SEM can reflect the force required for the human to drive the electric cylinder, that is, the error of the friction identification. For comparison, we repeated the above experiments, but use three different friction force compensation strategies: no compensation, with constant force compensation, and with function friction compensation obtained from the above friction identification in Section III. The compression force of the SEM during the experiment are shown in Fig.16.

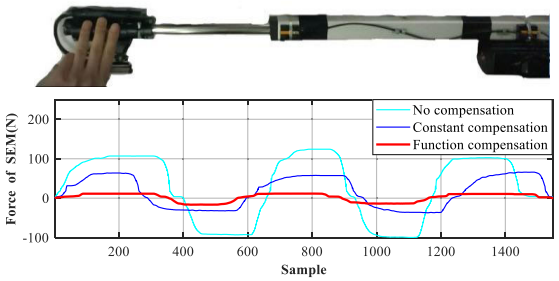

FIGURE 16. The compression force of SEM during friction compensation experiment. The maximum compression force is 124.2N without friction compensation. And it is 66N and 16N with friction compensation of constant value and identified function respectively.

From the results of the above-mentioned friction compensation experiments, it can be seen that the friction force of the electric cylinder is large when no friction compensation is performed, and the situation is significantly improved after the functional friction compensation is added. Meanwhile, the effect of functional friction compensation is much better than constant friction compensation.

The compression amount of the SEM reaches the maximum value when the speed is zero, that is when the movement of electric cylinder is reversed. According to the analysis, the compression amount of the SEM at this time is composed of two parts: (1) the error of the friction identification of the electric cylinder (2) the inertia force of the moving part of the electric cylinder.

C. SWING PHASE FOLLOWING EXPERIMENT

In order to verify the effect of the swing phase control algorithm, a one-leg reciprocating experiment was performed. The wearer secures the foot and the exoskeleton shoe and swings the leg back and forth at a speed of approximately 0.3 m/s. When the leg is in the swing phase, the target force at the end of the chain of parallel structure is 0. Under ideal conditions, the exoskeleton's leg will perfectly follow the wearer's leg, that is, the compression of the SEM is always 0 during the experiment. So the amount of compression of

the SEM during the process is the error of the exoskeleton's leg following the wearer, and can represent the magnitude of human-machine interaction force and the effect of swing phase control strategy during the experiment. Then compression amount of the SEM can reflect the magnitude of human-machine interaction force, which can represent the quality of the control effect.

Applying three kinds of control algorithms including PID, above-mentioned sliding mode control law without disturbance observer and above-mentioned sliding mode control law with disturbance observer, we carried out a phase following experiment.

With PID control algorithm, the control block diagram of each chain is shown in Fig.17.

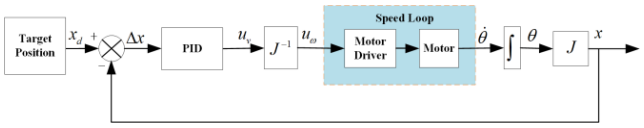

FIGURE 17. Control block diagram of PID control algorithm.

The control strategy of exoskeleton used for swing legs is position closed-loop control with speed internal loop, the velocity internal loop is integrated into motor driver, and the position error is measured by series elastic module. The PID control algorithm is used to calculate the speed instruction to the motor driver in real time by error.

During the experiment, compression force of the SEM is obtained, as shown in the Fig.18.

In Fig. 18, we can see that the magnitude of interaction force between wearer and exoskeleton using PID control algorithm and the one using sliding mode control algorithm without disturbance observer have little difference. But when the sliding mode control law based on disturbance observer is applied, the magnitude interaction force is the smallest, between −7.7N and 7N, which proves that the above sliding mode control based on disturbance observer makes the system have better following performance in the swing phase.

D. SQUATTING WITH LOAD EXPERIMENT

To verify the effect of PALExo in the stance phase, we conducted a squatting experiment. Letting the exoskeleton shoes directly support the ground, the wearer wears the exoskeleton on the upper body. A weight scale that transfers data to a computer in real-time is placed under the wearer's feet. Positional relationship between wearer, exoskeleton and weight scale during squatting experiment is shown in Fig.19. Because the weight scale shows the force on the wearer's feet, that is, the force carried by the wearer and the wearer's own weight. By subtracting the wearer's weight from the number on the scale, we can get the actual weight that the wearer is bearing on the upper body.

The wearer performs a squat action with a frequency of approximately 0.5 Hz. In the case where the exoskeleton bears 0kg, 25kg, 45kg, 66kg, the reading on the scale of the wearer is recorded, that is, the pressure on the wearer and

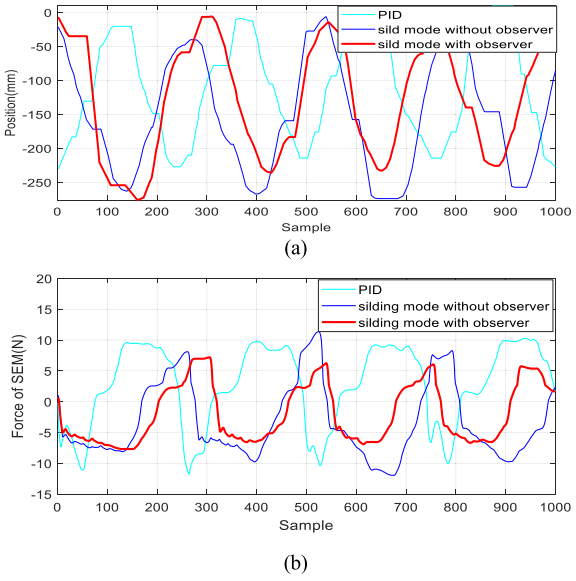

FIGURE 18. The result of the swing phase experiment with three kinds of control algorithms. (a) The position curve of swings. (b) Compression force of the SEM. When the sliding mode control law based on disturbance observer is applied, the compression force of the SEM is the smallest, between −7.7N and 7N, which proves that the above sliding mode control based on disturbance observer makes the system have better following performance in the swing phase.

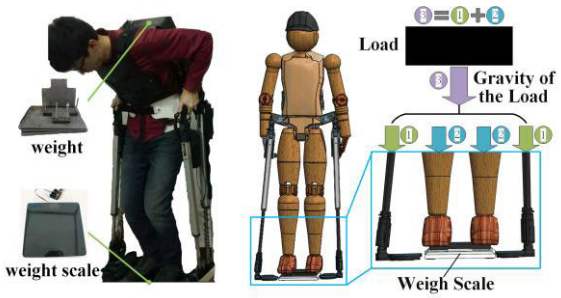

FIGURE 19. Positional relationship between wearer, exoskeleton and weight scale during squatting experiment.

the weight of the wearer (the wearer's weight is 79kg). The experimental results are shown in Fig.20.

It can be seen from (a) of Fig.20 that during the squatting process with different weights, the pressure on the wearer is basically unchanged, and the average value of the scale is 85.155kg when the weight is 0kg, 85.706kg when the weight is 25kg, 82.200kg when the weight is 45kg, and 86.851kg when the weight is 66kg. It means that the weight is mainly absorbed by the exoskeleton during the squatting process. For example, when the weight is 66kg, the wear only bears 7.25kg. When carrying 66kg weight, the force on the wearer's feet is 86.851kg, then the weight that the wear bearing is about 86.851-79 ≈ 7.25kg.

In contrast to the process of squatting with the exoskeleton, the wearer does not carry heavy loads to squat without the exoskeleton. The pressure on the sole of the foot and the one when the exoskeleton is worn are shown in (b) of Fig.20.

When the exoskeleton is not worn, the average pressure of the sole is 79.548kg, and when the exoskeleton is worn,

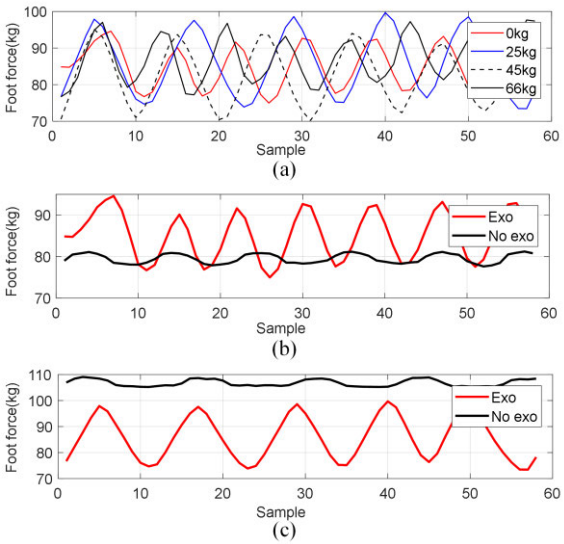

FIGURE 20. The result of the squatting experiment. (a) The pressure on the wearer carrying different weights with the exoskeleton. (b) The pressure on the wearer carrying 0kg with exoskeleton and without the exoskeleton. (c) The pressure on the wearer carrying 25kg with the exoskeleton and without the exoskeleton.

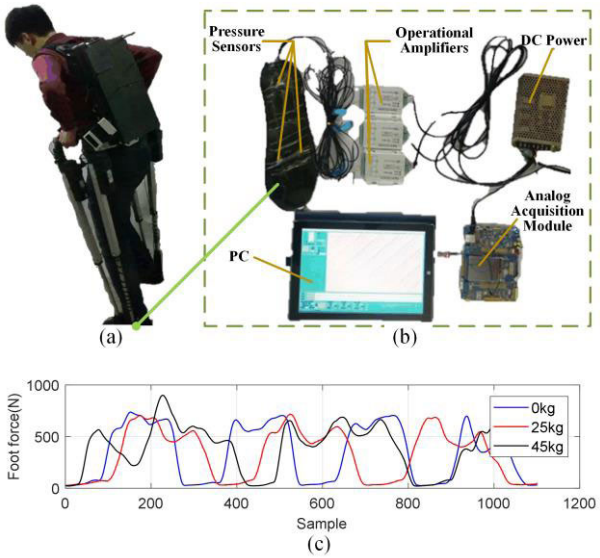

FIGURE 21. Walking experiment (a) Experimental process. (b) Experimental data acquisition system (c) The pressure on the wearer carrying different weights with exoskeleton.

it is 85.155kg. It shows that the exoskeleton has a certain influence on the wearer's squatting process, which will give the wearer some pressure.

The wearer carries a weight of 25kg to squat, the pressure on the sole of the foot and the one with wear wearing exoskeleton are shown in (c) of Fig.20.

When the exoskeleton is not worn, the average pressure of the sole is 106.791kg, and when the exoskeleton is worn, it is 85.706kg. It can be seen that the exoskeleton has a certain boosting effect during the squatting process.

E. WALKING WITH LOAD EXPERIMENT

In order to verify the load performance of the exoskeleton when walking, we proceeded walking experiments with 0kg, 25kg and 45kg weight respectively at speeds of about 2km/h. The right foot pressure of wearer is recorded by a pressure measuring insole. The results are shown in Fig.21.

The experimental result shows that when wearer walking with different weights, the pressure on the wearer has no obvious change. And it can be seen that when the leg switches from the swing phase to the stance phase, there is a sudden change in sole pressure. These phenomena indicate that the exoskeleton has a certain weight-reducing effect when walking, but there are certain problems in the excessive process when the legs switching between the swinging phase and the stance phase.

V. CONCLUSION

The parallel lower limb exoskeleton system PALExo introduced above is meant to enhance the human capacity of bearing weight. The parallel structure brings PALExo some benefits, such as good loading performance, wearing comfortableness and adaptability to different heights of the wearers. Owing to the innovative series elastic module (SEM) with multi-segment stiffness, PALExo is compliant and comfortable for the wearer. The control strategy of the stance leg and swing leg is unified as the target force control of SEM. Differently, the target force is zero for swinging leg, and it is calculated by dynamic model for stance leg. In order to add robustness to stabilize PALExo against the uncertainties from wearer and environment, we select sliding mode control based on the nominal model to track the target force. Disturbance observer is introduced to reduce the impact of disturbance such as modeling errors and other slow time-varying disturbance. Based on the LuGre friction model and parameter identification by genetic algorithm(GA), the friction of electric cylinders is compensated, which improves the response performance of the system. Finally, a series of experiments under different conditions are carried out, the rationality and the power-assisted effect of PALExo are verified. The test results show that PALExo plays a positive role when bearing weight. But it also shows that there are some deficiencies in current systems. For example, there is an impact in the switching phase between the swing phase and the stance phase, and it is difficult to balance PALExo when walking with weight.

Our future work may include several points: (1) Integrating pressure sensors into the shoes and using the sole pressure value in control method. (2) applying various methods including EMG signals and metabolism of wearer for experiments to reflect the full impact of the exoskeleton on the wearer. (3) studying the dynamic characteristics of the exoskeleton in the process of switching between the stance phase and the swing phase to improve walking characteristics with weight.

REFERENCES

[1] T. Yan, M. Cempini, C. M. Oddo, and N. Vitiello, "Review of assistive strategies in powered lower-limb orthoses and exoskeletons," *Robot. Auto. Syst.*, vol. 64, pp. 120–136, Feb. 2015.

[2] A. M. Dollar and H. Herr, "Lower extremity exoskeletons and active orthoses: Challenges and state-of-the-art," *IEEE Trans. Robot.*, vol. 24, no. 1, pp. 144–158, Feb. 2008.
[3] H. Herr, "Exoskeletons and orthoses: Classification, design challenges and future directions," *J. NeuroEng. Rehabil.*, vol. 6, no. 1, pp. 1–9, Dec. 2009.
[4] G. J. Dick and E. A. Edwards, "Human bipedal locomotion device," U.S. Patent 5 016 869, May 21, 1991.
[5] A. Bock, "Device for helping a person to walk," U.S. Patent 6 719 671, Apr. 13, 2004.
[6] C. Mahon. *Watch a Man Run 24 MPH Using the Bionic Boots He Invented Himself*. Accessed: Nov. 6, 2017. [Online]. Available: https://www.outerplaces.com/science/item/17000-bionic-boots-keahi-seymour-video
[7] J. Vance and J. A. Mercer, "Impact forces during running in a novel spring boot," in *Proc. 25th Annu. Conf. Amer. Soc. Biomech.*, 2001, pp. 1–3.
[8] A. B. Zoss, H. Kazerooni, and A. Chu, "Biomechanical design of the Berkeley lower extremity exoskeleton (BLEEX)," *IEEE/ASME Trans. Mechatronics*, vol. 11, no. 2, pp. 128–138, Apr. 2006.
[9] H. Kazerooni and R. Steger, "The Berkeley lower extremity exoskeleton," *J. Dyn. Syst., Meas., Control*, vol. 128, no. 1, pp. 14–25, Sep. 2005.
[10] A. Chu, H. Kazerooni, and A. Zoss, "On the biomimetic design of the Berkeley lower extremity exoskeleton (BLEEX)," in *Proc. IEEE Int. Conf. Robot. Autom.*, Barcelona, Spain, Apr. 2005, pp. 4345–4352.
[11] L. Martin. *Human Universal Load Carrier (HULC)*. Accessed: Apr. 1, 2019. [Online]. Available: http://www.army-technology.com/projects/human-universal-load-carrier-hulc/
[12] Y. Sankai, "HAL: hybrid assistive limb based on cybernics," in *Robotics Research*, vol. 66. Berlin, Germany: Springer, 2011, pp. 25–34.
[13] K. Suzuki, G. Mito, H. Kawamoto, Y. Hasegawa, and Y. Sankai, "Intention-based walking support for paraplegia patients with robot suit HAL," *Adv. Robot.*, vol. 21, no. 12, pp. 1441–1469, Jan. 2007.
[14] Raytheon Company. *Raytheon XOS 2 Exoskeleton, Second-Generation Robotics Suit*. Accessed: Apr. 1, 2019. [Online]. Available: https://www.army-technology.com/projects/raytheon-xos-2-exoskeleton-us/
[15] A. Chiri, M. Cempini, S. M. M. De Rossi, T. Lenzi, F. Giovacchini, N. Vitiello, and M. C. Carrozza, "On the design of ergonomic wearable robotic devices for motion assistance and rehabilitation," in *Proc. Annu. Int. Conf. IEEE Eng. Med. Biol. Soc.*, San Diego, CA, USA, Aug. 2012, pp. 6124–6127.
[16] C. W. Radcliffe, "Four-bar linkage prosthetic knee mechanisms: Kinematics, alignment and prescription criteria," *Prosthetics Orthotics Int.*, vol. 18, no. 3, pp. 159–173, Dec. 1994.
[17] D. J. Hyun, H. Park, T. Ha, S. Park, and K. Jung, "Biomechanical design of an agile, electricity-powered lower-limb exoskeleton for weight-bearing assistance," *Robot. Auto. Syst.*, vol. 95, pp. 181–195, Sep. 2017.
[18] *RB3D_BrochureEXO_HV3_EN_L*, RB3D, Moneteau, France, 2014.
[19] J. Ashihara, Y. Ikeuchi, H. Kudoh, Y. Hiki, T. Noda, and T. Koshiishi, "Walking assist device," U.S. Patent 8 267 886, Sep. 18, 2012.
[20] J.-P. Merlet, "Structural synthesis and architectures," in *Parallel Robots*, vol. 128, 2nd ed. Berlin, Germany: Springer, 2006, pp. 19–26.
[21] H. D. Taghirad, "Robot classification," in *Parallel Robots: Mechanics and Control*. Boca Raton, FL, USA: CRC press, 2013, pp. 10–18.
[22] G. Gogu, "Structural parameters," in *Structural Synthesis of Parallel Robots*, vol. 866. Berlin, Germany: Springer, 2008, pp. 31–127.
[23] O. Khatib, "Augmented object and reduced effective inertia in robot systems," in *Proc. Amer. Control Conf.*, Atlanta, GA, USA, Jun. 1988, pp. 2140–2147.
[24] J. Hunt, H. Lee, and P. Artemiadis, "A novel shoulder exoskeleton robot using parallel actuation and a passive slip interface," *J. Mech. Robot.*, vol. 9, no. 1, pp. 1–7, Feb. 2017.
[25] A. Gupta, M. K. O'Malley, V. Patoglu, and C. Burgar, "Design, control and performance of ricewrist: A force feedback wrist exoskeleton for rehabilitation and training," *Int. J. Robot. Res.*, vol. 27, no. 2, pp. 233–251, Feb. 2008.
[26] A. Roy, H. I. Krebs, S. L. Patterson, T. N. Judkins, I. Khanna, L. W. Forrester, R. M. Macko, and N. Hogan, "Measurement of human ankle stiffness using the anklebot," in *Proc. IEEE 10th Int. Conf. Rehabil. Robot.*, Noordwijk, The Netherlands, Jun. 2007, pp. 356–363.
[27] J. Klein, S. Spencer, J. Allington, J. E. Bobrow, and D. J. Reinkensmeyer, "Optimization of a parallel shoulder mechanism to achieve a high-force, low-mass, robotic-arm exoskeleton," *IEEE Trans. Robot.*, vol. 26, no. 4, pp. 710–715, Aug. 2010.
[28] Z. Guoan, "Research on hybrid-drive fukk body powered exoskeleton robot," Ph.D. dissertation, Harbin Inst. Technol., Harbin, China, 2018.

TIANSHUO WANG received the B.S. degree in mechanical engineering from the Harbin Institute of Technology (HIT), Harbin, China, in 2015, where he is currently pursuing the Ph.D. degree with the School of Mechatronics Engineering.

His research interests include robotic exoskeletons, parallel robots, and continuum robots.

YANHE ZHU (Member, IEEE) received the B.S. and Ph.D. degrees in mechatronics engineering from the Harbin Institute of Technology (HIT), Harbin, China, in 1998 and 2004, respectively.

He is currently a Professor and a Ph.D. Supervisor with the School of Mechatronics Engineering, HIT. He is also the Deputy Director of the State Key Laboratory of Robotics and System. His research interests include reconfigurable modular robots and robotic exoskeletons.

TIANJIAO ZHENG received the B.S. and M.S. degrees in mechanical engineering from the Harbin Institute of Technology (HIT), Harbin, China, in 2012 and 2014, respectively, where he is currently pursuing the Ph.D. degree with the School of Mechatronics Engineering.

His research interests include nonlinear dynamics, wearable rehabilitation robots, and bionic robots.

DONGBAO SUI received the B.S. degree in mechanical engineering and automation from the Beijing University of Posts and Telecommunications, Beijing, China, in 2015. He is currently pursuing the Ph.D. degree with the School of Mechatronics Engineering, Harbin Institute of Technology.

His research interests include continuum robots and robotic exoskeletons.

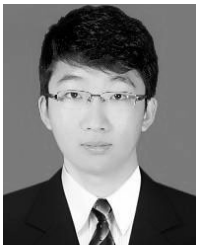

SIKAI ZHAO received the B.S. degree in mechanical engineering from the Harbin Institute of Technology (HIT), Harbin, China, in 2013, where he is currently pursuing the Ph.D. degree with the School of Mechatronics Engineering.

His research interests include robotic exoskeletons and bionic robots.

JIE ZHAO (Member, IEEE) received the B.S. and Ph.D. degrees in mechatronics engineering from the Harbin Institute of Technology (HIT), Harbin, China, in 1990 and 1996, respectively.

He is currently a Professor and a Ph.D. Supervisor with the School of Mechatronics Engineering, HIT. He is also the Leader of the Subject Matter Expert Group of Intelligent Robot in National Key Research and Development Program supervised by the Ministry of Science and Technology of China. His research interests include design, modeling, and control of bionic robots and industrial robots.